IEEE Access
Multidisciplinary | Rapid Review | Open Access Journal

Received March 27, 2022, accepted April 8, 2022, date of publication April 25, 2022, date of current version May 4, 2022.

Digital Object Identifier 10.1109/ACCESS.2022.3169605

A Study of Microwave Ablation With Hollow Antenna

SONGHUA JIN AND QIANG WANG
School of Information Science and Technology, Nantong University, Nantong 226000, China
Corresponding author: Qiang Wang (wang_q@ntu.edu.cn)

This work was supported by the Key University Science Research Project of Jiangsu Province, China under Grant 19KJ320004.

ABSTRACT Most microwave ablation antennas produce a non-spherical ablation zone. We propose a hollow microwave ablation antenna. In the hollow antenna, we use a hollow copper tube as the inner conductor. Compared with the copper core coaxial antenna, the hollow antenna reduces the current on the surface of the outer conductor and produces a spherical ablation zone. We use an internal L-type matching network to design the impedance matching of the hollow antenna. We fabricated the hollow antenna and did the ablation experiments in egg white to verify the ablating ability. The experimental results are similar to the simulated results. The roundness of the ablation zone reaches 86 % at an input power of 20 W and a duration time of 600 s, which shows the ability of the hollow antenna to produce a spherical ablation zone. The hollow antenna can increase the accuracy of microwave ablation and reduce the damage to the normal tissues.

INDEX TERMS Microwave ablation antenna, ablation zone, matching network, roundness.

I. INTRODUCTION

Malignant tumor, a well-known malignant disease, has a high rate of incidents and mortality. Currently, tumor treatments include surgery, chemotherapy, and radiotherapy [1]. However, these treatments have certain limitations. They rarely treat cancer patients at metaphases or terminals. Meanwhile, they may induce multiple complications, which may increase the risk of deteriorating and accelerating the death of patients.

Thermal ablation, a promising technology for tumor treatment, allows for low invasion. Image-guided thermal ablation heats the tumor to a cytotoxic temperature, which causes instantaneous cell death [2]. Approaches used for thermal ablation include focused ultrasound [3], radiofrequency [4], and microwave ablation [5]. The focused ultrasound ablation is a technology that focuses beams of ultrasound wave at one point, where the highest magnitude of energy is deposited [6]. The point rapidly reaches a cytotoxic temperature to kill tumor cells. However, due to the energy attenuation of the ultrasound wave, the ablation zone is small which does not meet the general requirements of thermal ablation. If doctors use long-term treatment, it will increase the risk of tissue damage. Therefore, doctors often apply focused ultrasound ablation to ablate tissues with good acoustic tissue properties, such as the uterus, prostate, maxillofacial area, and so on [7]. Radiofrequency ablation is a thermal therapy that uses the high-frequency oscillation current to kill tumor cells [8]. However, the electrical conductivity of tissues limits the application of radiofrequency ablation. Microwave ablation forms an electromagnetic field to heat tumors to death by the microwave [9], [10]. Compared with other ablations, microwave ablation has been widely used due to its high efficiency [11].

Because most tumors are nearly spherical shapes [12], researchers expect microwave ablation to produce a spherical ablation zone. It is important for microwave ablation antennas in clinical applications. To date, several types of microwave ablation antennas have been proposed to achieve a spherical ablation zone for tumor treatments [13], [14]. However, in previous studies, the researchers only considered improving the sleeve or choke of antennas to increase the roundness of the ablation zone, but such designs may cause larger invasion.

In this study, we propose a hollow antenna with water cooling, which can produce a spherical ablation zone and reduce the damage to the normal tissues. We use an internal L-type matching network to design the impedance matching of the hollow antenna. We simulate the specific absorption rate (SAR) patterns, temperature distribution, and ablation zone by HFSS and Fluent. We did experiments in egg white which verified the simulated results.

II. ANTENNA DESIGN AND SIMULATION

A. ANTENNA DESIGN

Fig. 1 shows two structures of microwave ablation antennas with water-cooling. All antennas are fed with a coaxial

The associate editor coordinating the review of this manuscript and approving it for publication was Tutku Karacolak.

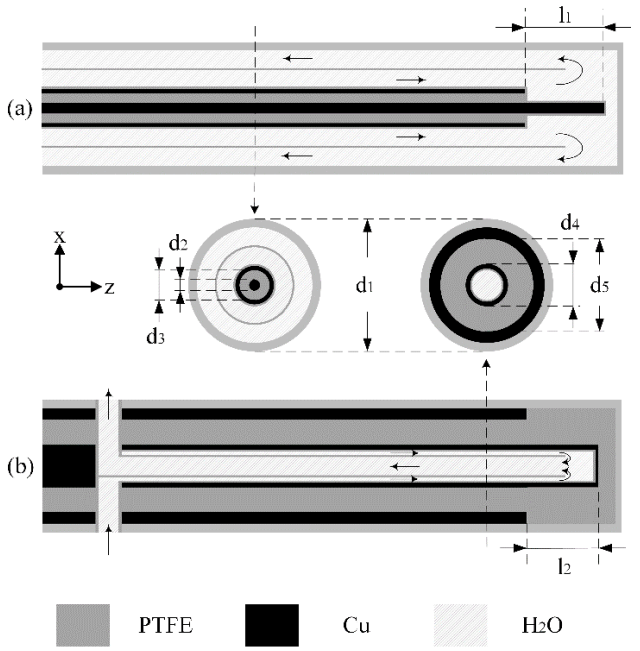

FIGURE 1. Structures of the microwave ablation antenna. (a) coaxial antenna, (b) hollow antenna.

TABLE 1. Dimensions of antennas.

Symbol	Unit	Value
l_1	mm	12.3
l_2	mm	9.0
d_1	mm	5.5
d_2	mm	0.3
d_3	mm	1.0
d_4	mm	1.2
d_5	mm	4.0

cable and designed to operate at 2.45 GHz. There are four advantages of this frequency over lower frequencies (e.g. 915 MHz), including shorter radiating part, high round SAR pattern, good heating capability, and large ablation zone [15].

Fig. 1(a) shows the structure of a coaxial microwave ablation antenna. The coaxial antenna uses a copper core as the inner conductor of the antenna with the cooling water outside it. Fig. 1(b) shows the structure of a hollow microwave ablation antenna. The hollow antenna uses a hollow copper tube instead of the copper core as the inner conductor with the cooling water inside the tube. In Fig. 1, gray, black, and white represent polytetrafluoroethylene (PTFE), copper, and water, respectively. Table 1 shows the dimensions of the two antennas.

B. ELECTROMAGNETIC SIMULATION

We choose egg white as the experimental material because of its similar characteristics to the hepatocyte. Meanwhile, due to its high transparency, we can easily monitor the formation

TABLE 2. Parameter of hepatocyte and egg white.

Symbol	Unit	hepatocyte	Egg white
ε	-	47.6	66.7
σ	S/m	2.18	1.92
ρ	kg/m^3	1070	1041
c	J/(kg·°C)	3700	3800
K	W/(m^2·°C)	0.535	0.55

process of the ablation zone [16]. Table 2 shows the characteristics of egg white and hepatocyte.

Fig. 2 shows the simulated model of the antenna. The height and diameter of the model are 80 mm and 60 mm, respectively, and the insertion depth of the antenna is 60 mm. The coaxial antenna and hollow antenna are all water-cooled. Therefore, a convection boundary condition is applied at the antenna/egg white interface and outer boundaries of the egg white [17]. The flow rate and temperature of the cooling water determine the heating exchange efficiency.

Normal saline is used as cooling water to reduce the front temperature of the microwave ablation antenna. Even if cooling water leaks, it will not affect the body fluid balance. But conductive saline can block electromagnetic radiation and reduce the ablation zone. In the hollow antenna, normal saline in the tube cools the antenna, which can reduce the front temperature and increase the ablation zone.

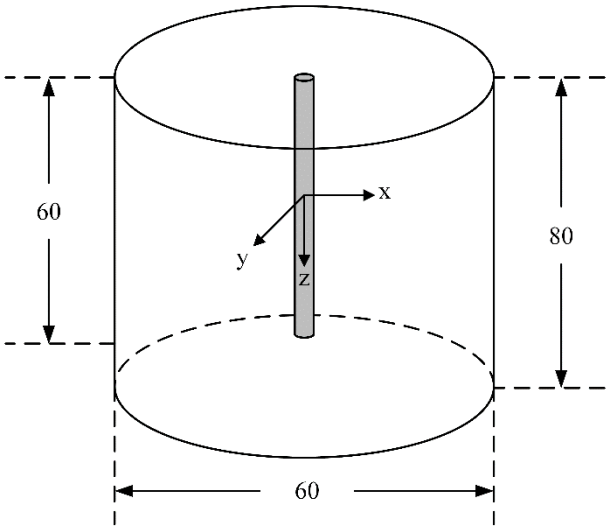

FIGURE 2. Model of the microwave ablation antenna. (unit: mm).

The heat generated in egg white (Q_e) is calculated [18] by

$$Q_e = \rho SAR \tag{1}$$

where ρ is the density of the egg white (kg/m^3), and SAR is the specific absorption rate of the egg white (W/kg).

The SAR is calculated by

$$SAR = \frac{\sigma}{2\rho} E^2 \tag{2}$$

where σ is the conductivity of the egg white (S/m), and E is the electric field intensity in egg white (V/m).

Therefore

$$Q_e = \frac{\sigma}{2}E^2 \tag{3}$$

Fig. 3 shows the simulated SAR patterns of the coaxial antenna and hollow antenna normalized to the maximum value by HFSS. The SAR pattern of the hollow antenna is larger in diameter. The SAR pattern of the coaxial antenna is like a comet, which may be caused by the backward diffusion of the current on the conductor surface along the outer conductor surface.

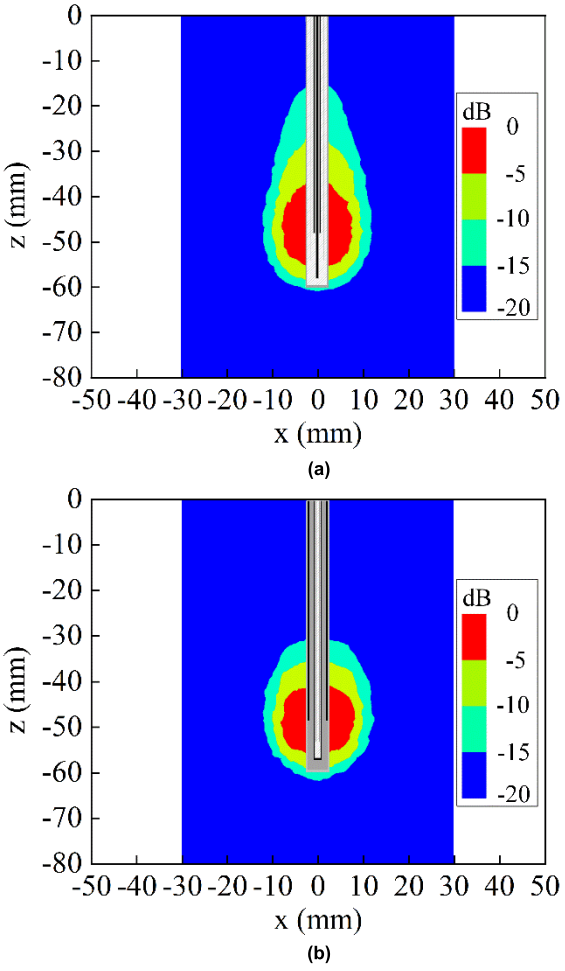

FIGURE 3. Simulated SAR patterns of the two antennas. (a) coaxial antenna, (b) hollow antenna.

The electric field distribution of the egg white around the antenna [19] is

$$E = \frac{J}{2\pi}e^{-jkr}\left(\frac{\eta}{r^2}+\frac{1}{j\omega\varepsilon^* r^3}\right)\cos\theta\hat{r} + \frac{J}{4\pi}e^{-jkr}\left(\frac{j\omega\mu}{r}+\frac{\eta}{r^2}+\frac{1}{j\omega\varepsilon^* r^3}\right)\sin\theta\hat{\theta} \tag{4}$$

where J is the current density (A/m^2), k, η, and $\varepsilon*$ are the inherent characteristics of the egg white, r is the distance from the inner conductor in the antenna (m), and θ is the angle between the observation vector and the axial direction.

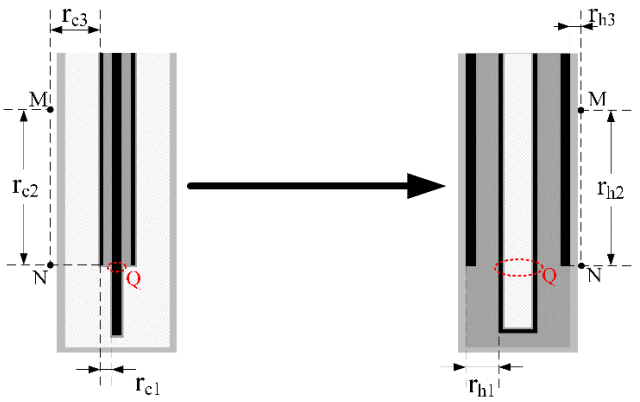

FIGURE 4. Design principle of the hollow antenna.

The current density is related to the diameter (d) of the inner conductor,

$$J = \frac{I}{k_s d} \tag{5}$$

where k_s is the antenna coefficient. The skin effect causes the current of the antenna to concentrate on the conductor surface, so k_s remains approximately constant.

Therefore

$$E_M = \frac{I}{2\pi k_s d}e^{-jkr}\left[\frac{j\omega\mu}{r}\sin\theta\hat{\theta}+\left(\frac{\eta}{r^2}+\frac{1}{j\omega\varepsilon^* r^3}\right)\times\left(2cos\theta\hat{r}+\sin\theta\hat{\theta}\right)\right] \tag{6}$$

Fig. 4 shows the design principle of the hollow antenna. In Fig. 4, point M represents a rear point at the antenna/egg white interface, and point N is the projection of the top of the outer conductor at the antenna/egg white interface. According to the paper [20], position Q in Fig. 4 is the location where the radiation intensity is the strongest. So

$$\begin{cases} r_{c-M} = r_{c1} + \sqrt{r_{c2}^2 + r_{c3}^2} \\ r_{h-M} = r_{h1} + \sqrt{r_{h2}^2 + r_{h3}^2} \end{cases} \tag{7}$$

$$\begin{cases} r_{c-N} = r_{c1} + r_{c3} \\ r_{h-N} = r_{h1} + r_{h3} \end{cases} \tag{8}$$

where r_{c-M} and r_{h-M} are the minimum distances from position Q of the coaxial antenna and hollow antenna to point M, respectively. Where r_{c-N} and r_{h-N} are the minimum distances from position Q of the coaxial antenna and hollow antenna to point N, respectively.

According to Table 1,

$$\begin{cases} r_{c1} < r_{h1} \\ r_{c2} = r_{h2} \\ r_{c3} > r_{h3} \end{cases} \tag{9}$$

$$r_{c1} + r_{c3} + \frac{d_2}{2} = r_{h1} + r_{h3} + \frac{d_4}{2} = d_1 \tag{10}$$

Therefore

$$r_{c-N} > r_{h-N} \tag{11}$$

$$\begin{cases} r_{c-M} < r_{h-M}, & r_{h2} > r_0 \\ r_{c-M} = r_{h-M}, & r_{h2} = r_0 \\ r_{c-M} > r_{h-M}, & r_{h2} < r_0 \end{cases} \tag{12}$$

where $r_0 \approx 3.59$ mm.

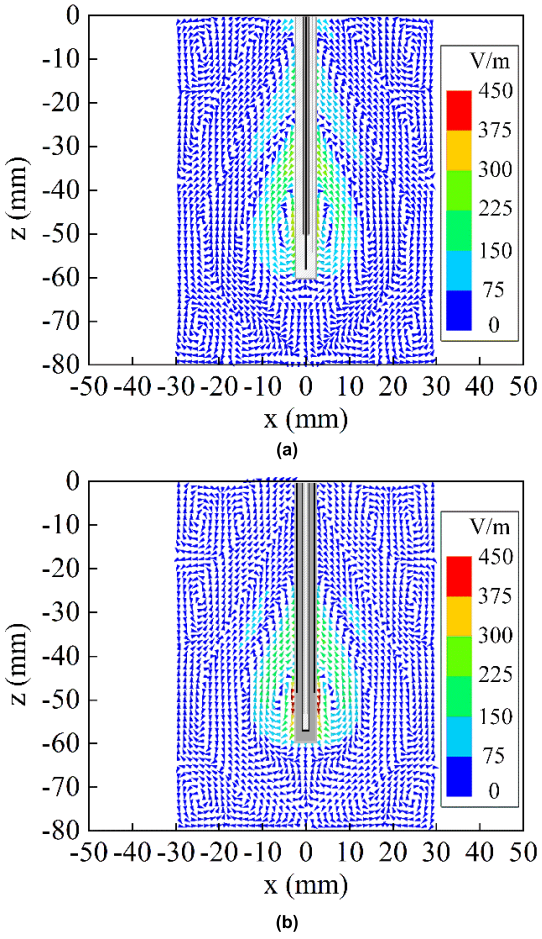

FIGURE 5. Simulated electric field direction and intensity for two structures. (a) coaxial antenna, and (b) hollow antenna.

According to (6), (11), and (12), the SAR pattern of the hollow antenna shrinks back along the antenna and increases outward in the direction of the vertical antenna. Compared with the coaxial antenna, the SAR pattern of the hollow antenna is close to the round shape.

Fig. 5 shows the electric field direction and intensity for two antennas. The electric field of the hollow antenna is concentrated in the front end, which optimizes the property of the antenna.

C. MATCHING NETWORK

In the antenna design, we need a smaller S11-parameter (dB) which can deposit a higher microwave power into egg white. Fig. 6 shows the S11 of the hollow antenna. The S11 of the hollow antenna at 2.45 GHz is only −2.65 dB, due to the impedance mismatch between the hollow antenna and the coaxial cable.

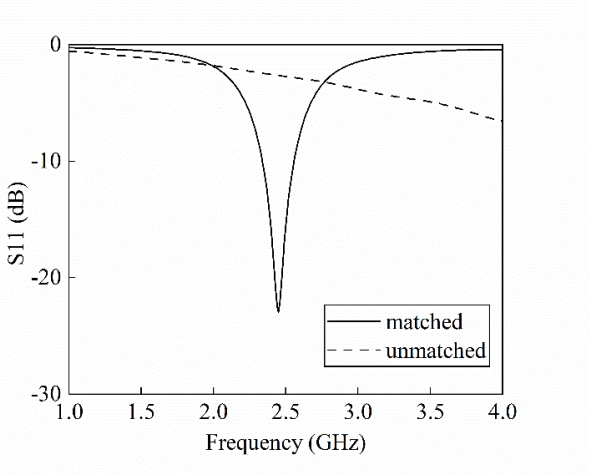

FIGURE 6. S11 of the hollow antenna.

Fig. 7 shows the internal matching network of the hollow antenna. The matching network used is the L type one, which is equivalent to an inductor and a resistor in series with a parallel capacitor [21]. We can obtain a larger capacitance by decreasing the inner diameter of the outer conductor of the coaxial cable, which decreases the impedance of the matching network. On the other hand, we can acquire a larger inductance by removing the dielectric spacer between the two conductors of the coaxial cable, which increases the impedance of the matching network.

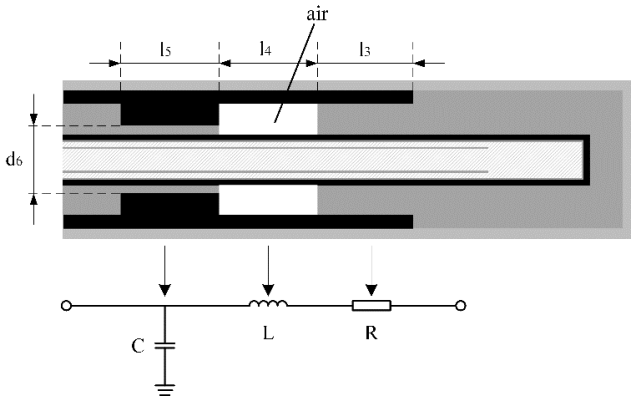

FIGURE 7. The matching network of the hollow antenna.

The l_5 and l_4 determine the value of the capacitor (C) and inductor (L), respectively. The C and L are calculated [5], [22], [23] by

$$C = l_5 \frac{2\pi\varepsilon}{ln\left(\frac{d_6}{d_4}\right)} \tag{13}$$

$$L = l_4 \frac{\mu}{2\pi} ln\left(\frac{d_5}{d_4}\right) \tag{14}$$

where ε is the dielectric constant of PTFE and μ is the permeability of air.

We fine-tune the dimensions of the L-type matching network by the HFSS to produce a low S11 of the antenna at 2.45 GHz. Table 3 shows the dimensions of the L-type matching network. After optimization, the corresponding S11 of the hollow antenna is −22.97 dB at 2.45 GHz, as shown in Fig. 6.

TABLE 3. Dimensions of the matching network.

Symbol	Unit	Value
l_3	mm	7
l_4	mm	10
l_5	mm	8
d_6	mm	0.8

D. THERMAL SIMULATION

We import the simulated SAR results of the antennas into Fluent as a thermal source for the thermal simulations. The initial temperature of the egg white and cooling water are 25 °.

Because the coaxial antenna and hollow antenna are axisymmetric, we can use the shape of the x-z plane to assess the shape of the ablation zone. Fig. 8 shows the temperature distributions of the coaxial antenna and hollow antenna at an input power of 20 W and a duration time of 600 s. We set the 60 °C temperature contour as the boundary of the ablation zone. The ablation zone in Fig. 8 coincides with the -15 dB SAR pattern in Fig. 3. The maximum temperature of the hollow antenna is higher than that of the coaxial antenna. This means the heating efficiency of the hollow antenna is higher. The ablation zone of the antenna is smoother than the SAR pattern because of thermal diffusion.

We introduce a parameter (R_{xz}) to assess the roundness of the ablation zone. The R_{xz} is defined as

$$R_{xz} = \begin{cases} \dfrac{d_x}{d_z}, & d_x < d_z \\ \dfrac{d_z}{d_x}, & d_x \geq d_z \end{cases} \tag{15}$$

where d_x is the length of the ablation zone in the x-direction, and d_z is the length of the ablation zone in the z-direction. When the R_{xz} is 100 % means the ablation zone is a round shape. When the R_{xz} is 0 % means the ablation zone is a line.

The R_{xz} of the coaxial antenna and hollow antenna are 72.16 % and 92.11 %.

Fig. 9 shows the temperature distributions of the hollow antenna at different input powers. For the hollow antenna, the ablation zones are similar at input power of 20 W and 30 W, the duration time of 600 s and 400 s, respectively. But the maximum temperature of the ablation zone is nearly 100 °C at which the egg white turns into carbon at a power of 30 W and a duration time of 400 s, at which the egg white turns into carbon. This restricts the antenna from radiating.

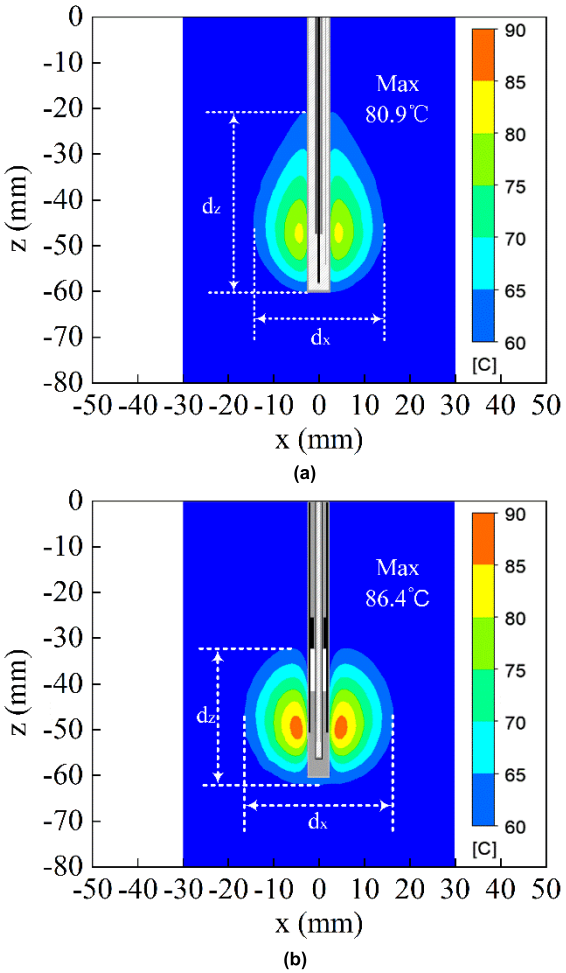

FIGURE 8. The temperature distributions at an input power of 20 W and a duration time of 600 s. (a) coaxial antenna, and (b) hollow antenna.

The temperature of the ablation zone gradually increases with increasing power.

Fig. 10 shows the temperature distributions of the hollow antenna at an input power of 20 W. The dimensions of the ablation zone are increasing with increasing duration time. The R_{xz} of the hollow antenna is 66.59 %, 94.34 %, 91.38 %, and 92.11 % at the duration time of 60 s, 180 s, 360 s, and 600 s, respectively, which show in Fig. 8 (b) and Fig. 10. The R_{xz} of the ablation zone is over 90 % when the duration time is over 180 s. The ablation zone is nearly a spherical shape.

III. MICROWAVE ABLATION EXPERIMENTS

According to our design, the hollow antenna was fabricated. Fig. 11 shows the fabricated antenna. The antenna was then put inside PTFE heat shrink and a heat gun was used to shrink the diameter of the heat shrink to 5.5 mm.

Fig. 12 shows the simulated and measured S11 of the hollow antenna in egg white. The S11 value of the simulated and measured results is a little offset. There may be two reasons: one is that the actual value is slightly different from the simulation setting value due to the temperature, and another is

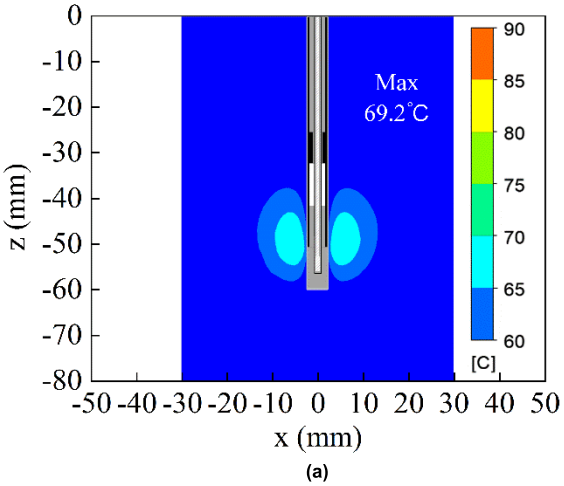

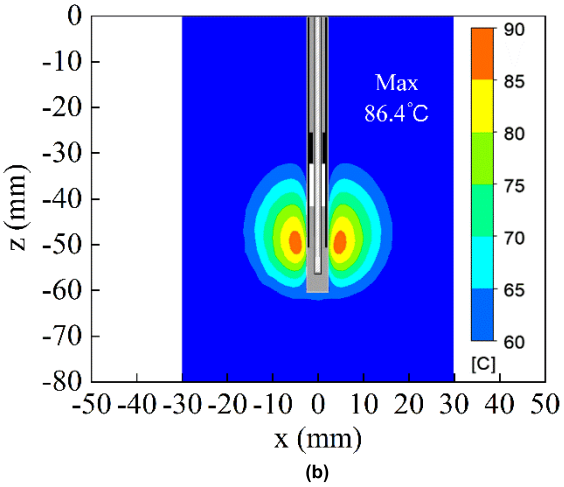

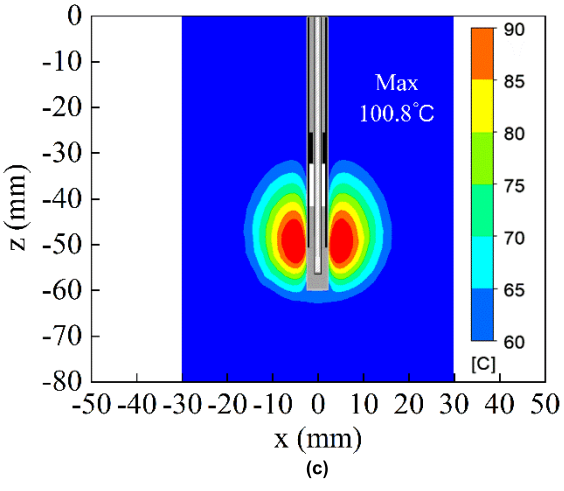

FIGURE 9. The temperature distributions of the hollow antenna. (a) 10 W, 1200 s, (b) 20 W, 600 s, and (c) 30 W, 400 s.

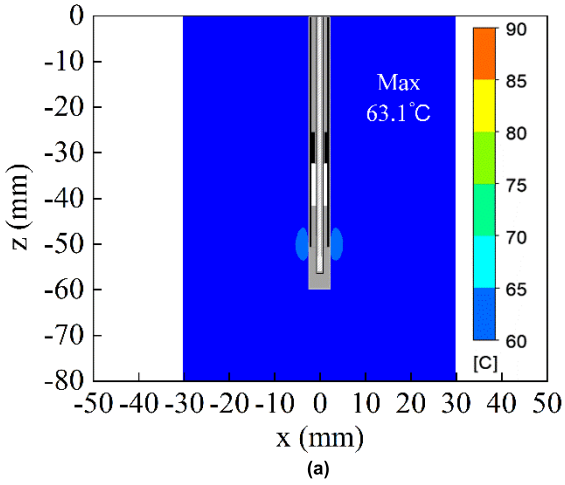

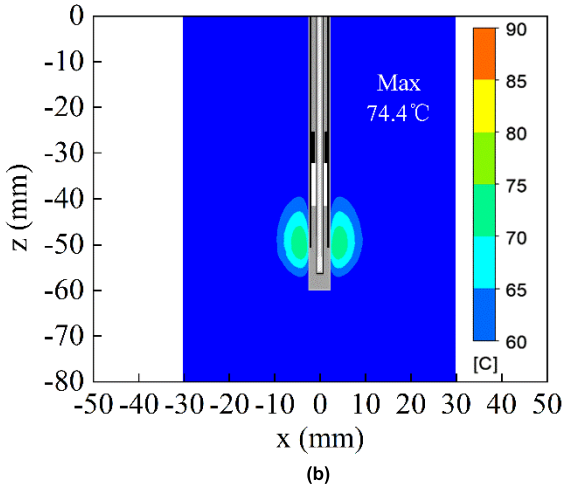

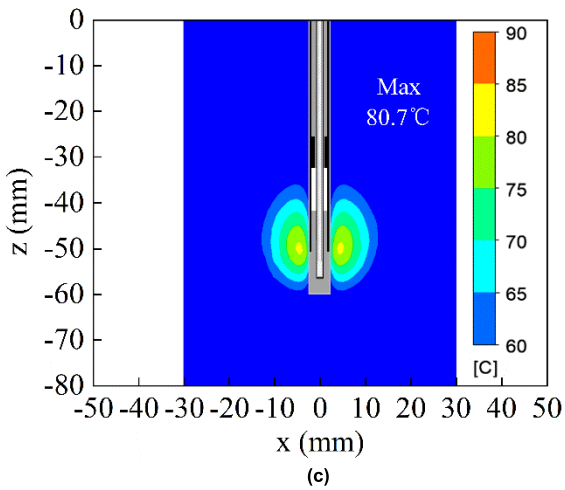

FIGURE 10. The temperature distributions of the hollow antenna at (a) 60 s, (b) 180 s, and (c) 360 s.

that the machining accuracy of the fabricated antenna hardly meets our requirements.

We do the ablation experiments at a signal of 2.48 GHz, an input power of 20 W, and a duration time of 600 s. Before and after the experiments, the S11 is −20.48 dB and −19.63 dB, respectively. The maximum reflected power of the antenna is less than 1 W during the experiments.

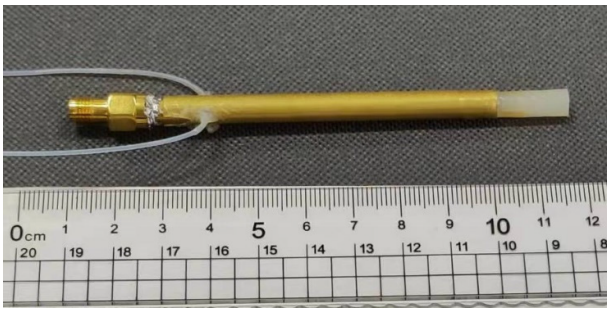

FIGURE 11. Photograph of the fabricated antenna.

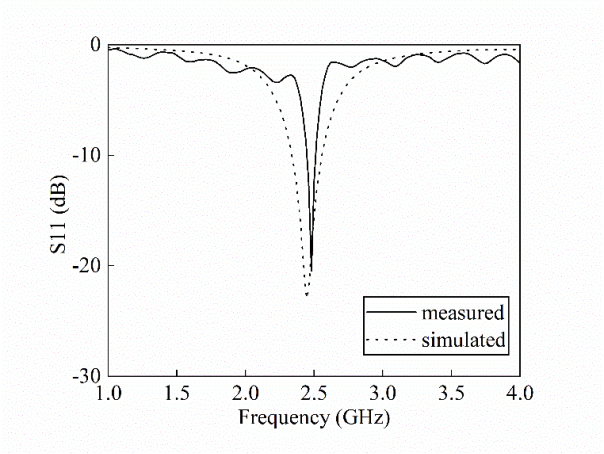

FIGURE 12. Simulated and measured S11 of the hollow antenna.

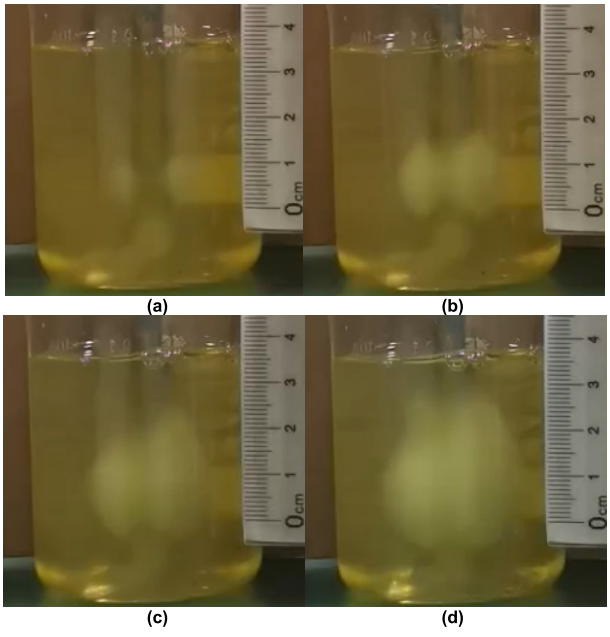

FIGURE 13. Photographs of the ablation experiments. (a) 60 s, (b) 180 s, (c) 360 s, and (d) 600 s.

Fig. 13 shows the experimental results at different times. With increasing time, the dimensions of the ablation zone become larger, and the shape of the ablation zone is close to spherical.

TABLE 4. Comparisons of microwave ablation antennas.

Antenna	Frequency (GHz)	d_x (mm)	d_z (mm)	R_{xz} (%)	Power (W)	Time (s)
Hollow antenna	2.45	29.9	34.8	86	20	600
Antenna one [24]	2.45	45.0	56.0	80	40	600
Antenna two [25]	6.00	30.0	38.0	79	20	600
Antenna three [26]	7.00	28.0	37.0	76	30	300
Antenna four [27]	1.90	32.8	58.0	57	20	600
Antenna five [28]	1.90	30.6	39.2	78	40	300

Table 4 shows the comparison of the hollow antenna and five microwave ablation antennas. From Table 4, we can find out that the R_{xz} of the hollow antenna reaches 86 %, indicating good ablation performance.

IV. CONCLUSION

In this study, the proposed antenna has a hollow structure producing a spherical ablation zone during microwave ablation. The design reduces the current on the surface of the outer conductor, which helps to form a spherical ablation zone. The measured results coincide with the simulated results. The R_{xz} of the fabricated antenna reaches 86 %, and the maximum temperature is less than 100 °C, which meets the requirements of clinical applications. The proposed hollow antenna has the potential of wide applications and developments in the medical field.

REFERENCES

[1] S. Thakkar, D. Sharma, K. Kalia, and R. K. Tekade, "Tumor microenvironment targeted nanotherapeutics for cancer therapy and diagnosis: A review," *Acta Biomaterialia*, vol. 101, pp. 43–68, Jan. 2020.
[2] M. Venturini, M. Cariati, P. Marra, S. Masala, P. L. Pereira, and G. Carrafiello, "CIRSE standards of practice on thermal ablation of primary and secondary lung tumours," *CardioVascular Interventional Radiol.*, vol. 43, no. 5, pp. 667–683, May 2020.
[3] V. Y. T. Cheung, "High-intensity focused ultrasound therapy," *Best Pract. Res. Clin. Obstetrics Gynaecol.*, vol. 46, pp. 74–83, Jan. 2018.
[4] N. J. Rommelfanger and G. Hong, "On the feasibility of wireless radio frequency ablation using nanowire antennas," *APL Mater.*, vol. 9, no. 7, pp. 1–9, Jul. 2021.
[5] H. Huang, L. Zhang, M. A. J. Moser, W. Zhang, and B. Zhang, "A review of antenna designs for percutaneous microwave ablation," *Phys. Medica*, vol. 84, pp. 254–264, Apr. 2021.
[6] K. Kaczmarek, T. Hornowski, B. Dobosz, and A. Józefczak, "Influence of magnetic nanoparticles on the focused ultrasound hyperthermia," *Materials*, vol. 11, no. 9, pp. 1–15, Sep. 2018.
[7] P. Rangraz, H. Behnam, and J. Tavakkoli, "Nakagami imaging for detecting thermal lesions induced by high-intensity focused ultrasound in tissue," *Proc. Inst. Mech. Eng., H, J. Eng. Med.*, vol. 228, no. 1, pp. 19–26, Jan. 2014.
[8] X. Sun, Z.-Z. He, Z.-S. Deng, Y.-X. Zhou, and J. Liu, "Liquid metal bath as conformable soft electrodes for target tissue ablation in radio-frequency ablation therapy," *Minimally Invasive Therapy Allied Technol.*, vol. 27, no. 4, pp. 233–241, Jul. 2018.
[9] H. Fallahi and P. Prakash, "Antenna designs for microwave tissue ablation," *Crit. Rev. Biomed. Eng.*, vol. 46, no. 6, pp. 495–521, Jan. 2018.
[10] S. Etoz and C. L. Brace, "Analysis of microwave ablation antenna optimization techniques," *Int. J. RF Microw. Comput.-Aided Eng.*, vol. 28, no. 3, pp. 1–9, Dec. 2017.

[11] F. Izzo, V. Granata, R. Grassi, R. Fusco, R. Palaia, P. Delrio, G. Carrafiello, D. Azoulay, A. Petrillo, and S. A. Curley, "Radiofrequency ablation and microwave ablation in liver tumors: An update," *Oncologist*, vol. 24, no. 10, pp. e990–e1005, Oct. 2019.

[12] P. Prakash, M. C. Converse, J. G. Webster, and D. M. Mahvi, "Design optimization of coaxial antennas for hepatic microwave ablation using genetic algorithms," in *Proc. IEEE Antennas Propag. Soc. Int. Symp.*, San Diego, CA, USA, Jul. 2008, pp. 1–4.

[13] M. M. Yassin, E. Tammam, A. A. Ibrahim, A. M. Said, and A. I. Galal, "A dual ring interstitial monopole antenna with spherical heating pattern for hepatic tumor microwave ablation," in *Proc. 36th Nat. Radio Sci. Conf. (NRSC)*, Port Said, Egypt, Apr. 2019, pp. 425–430.

[14] Z. A. Ibitoye, E. O. Nwoye, M. A. Aweda, A. A. Oremosu, C. C. Annunobi, and O. N. Akanmu, "Optimization of dual slot antenna using floating metallic sleeve for microwave ablation," *Med. Eng. Phys.*, vol. 37, no. 4, pp. 384–391, Apr. 2015.

[15] Y. Sun, Z. Cheng, L. Dong, G. Zhang, Y. Wang, and P. Liang, "Comparison of temperature curve and ablation zone between 915- and 2450-MHz cooled-shaft microwave antenna: Results in *ex vivo* porcine livers," *Eur. J. Radiol.*, vol. 81, no. 3, pp. 553–557, Mar. 2012.

[16] Y. Mohtashami, S. C. Hagness, and N. Behdad, "A hybrid slot/monopole antenna with directional heating patterns for microwave ablation," *IEEE Trans. Antennas Propag.*, vol. 65, no. 8, pp. 3889–3896, Aug. 2017.

[17] Y. Xu, M. A. J. Moser, E. Zhang, W. Zhang, and B. Zhang, "Large and round ablation zones with microwave ablation: A preliminary study of an optimal aperiodic tri-slot coaxial antenna with the π-matching network section," *Int. J. Thermal Sci.*, vol. 140, pp. 539–548, Jun. 2019.

[18] P. Phasukkit and T. Wongketsada, "Triple coaxial-half-slot antenna scheme with deep learning-based temperature prediction for hepatic microwave ablation: Finite element analysis and *in vitro* experiment," *IEEE Access*, vol. 9, pp. 79572–79587, 2021.

[19] S. Curto, M. Taj-Eldin, D. Fairchild, and P. Prakash, "Microwave ablation at 915 MHz vs 2.45 GHz: A theoretical and experimental investigation," *Med. Phys.*, vol. 42, no. 11, pp. 6152–6161, Nov. 2015.

[20] J. M. Bertram, D. Yang, M. C. Converse, J. G. Webster, and D. M. Mahvi, "A review of coaxial-based interstitial antennas for hepatic microwave ablation," *Crit. Rev. Biomed. Eng.*, vol. 34, no. 3, pp. 187–213, 2006.

[21] Y. Mohtashami, H. Luyen, J. F. Sawicki, J. D. Shea, N. Behdad, and S. C. Hagness, "Tools for attacking tumors: Performance comparison of triaxial, choke dipole, and balun-free base-fed monopole antennas for microwave ablation," *IEEE Antennas Propag. Mag.*, vol. 60, no. 6, pp. 52–57, Dec. 2018.

[22] H. Luyen, S. C. Hagness, and N. Behdad, "A balun-free helical antenna for minimally invasive microwave ablation," *IEEE Trans. Antennas Propag.*, vol. 63, no. 3, pp. 959–965, Mar. 2015.

[23] M. Ge, H. Jiang, X. Huang, Y. Zhou, D. Zhi, G. Zhao, Y. Chen, L. Wang, and B. Qiu, "A multi-slot coaxial microwave antenna for liver tumor ablation," *Phys. Med. Biol.*, vol. 63, no. 17, pp. 175011–175023, Sep. 2018.

[24] A. Z. Ibitoye, E. O. Nwoye, A. M. Aweda, A. A. Oremosu, C. C. Anunobi, and N. O. Akanmu, "Microwave ablation of *ex vivo* bovine tissues using a dual slot antenna with a floating metallic sleeve," *Int. J. Hyperthermia*, vol. 32, no. 8, pp. 923–930, Aug. 2016.

[25] H. Luyen, S. C. Hagness, and N. Behdad, "A minimally invasive coax-fed microwave ablation antenna with a tapered balun," *IEEE Trans. Antennas Propag.*, vol. 65, no. 12, pp. 7280–7287, Dec. 2017.

[26] H. Luyen, S. C. Hagness, and N. Behdad, "Reduced-diameter designs of coax-fed microwave ablation antennas equipped with baluns," *IEEE Antennas Wireless Propag. Lett.*, vol. 16, pp. 1385–1388, 2017.

[27] Y. Mohtashami, N. Behdad, and S. C. Hagness, "*Ex vivo* performance of a flexible microwave ablation antenna," *IEEE Trans. Biomed. Eng.*, vol. 68, no. 5, pp. 1680–1689, May 2021.

[28] Y. Mohtashami, N. Behdad, and S. C. Hagness, "Toward flexible microwave ablation antennas with a balun-free helical dipole design," *IEEE Trans. Antennas Propag.*, vol. 68, no. 7, pp. 5052–5060, Jul. 2020.

SONGHUA JIN was born in Zhoukou, China, in 1994. He received the Engineering degree from North China Electric Power University, in 2017. He is currently pursuing the M.S. degree with the School of Information Science and Technology, Nantong University. His research interest includes antenna design for microwave ablation.

QIANG WANG was born in Nantong, China, in 1978. He is currently working as an Associate Professor with the School of Information Science and Technology, Nantong University. His research interests include information and communication engineering, antenna design, and wireless communication.